First Principles Estimation of Shock Tube Tests on Nanoreinforced Composite Materials

Weiping Xu[1], Elizabeth K. Ervin[2]

[1]Lecturer, Civil Engineering, Southwest Jiaotong University, Room 402, Building C, 144 Jiaoda Road Southwest Jiaotong Science Park, Jinniu District Chengdu City, Sichuan Province, China 610031, Email: weipingxu2010@gmail.com

[2]Assistant Professor, Civil Engineering, 203 Carrier Hall, P.O. Box 1848, University, MS US 38677-1848, Email: eke@olemiss.edu

ABSTRACT

Extreme loads events can cause enormous human and infrastructure losses. Computer modeling is the key to reducing the high cost of dynamic monitoring and experimentation. Engineers in various fields have undertaken complicated modeling for structures under abnormal loads. However, an efficient and accurate model is necessary to more rapidly address dangerous shock problems. Composite materials have replaced metals in various applications thanks to their superior shock resistance properties. This investigation particularly relates to their usage on naval ships to achieve improved blast survivability with the additional benefit of lower cost. A relatively simple model is detailed for the approximate centerline response prediction of the specific complex case of composite materials tested in a shock tube. A modal analysis simulation of a beam is performed using gross properties as well as physical geometry and arbitrary shock. Closed form equations have been employed to derive the eigenproblem that generates mode shapes and natural frequencies, and the resulting responses are compared to experimental shock tube test results. The best outcome

was generated by the simplest model consisting of a shock pressure pulse averaged in two divisions and applied over the entire beam span. For this case, the simulation and experimental responses had reasonable correlation for fractured E-glass/vinyl-ester composite specimens with both nanoclay and graphite platelet reinforcement. This model is also a conservative estimate for the transient test deflection range for all other specimens.

Keywords closed-form, shock tube, composite, nanoreinforcement

1 INTRODUCTION

Extreme loads such as earthquakes and explosions can cause enormous human and infrastructure losses. Considering the high cost of dynamic monitoring and experimentation, computer models are the keys to reducing physical test requirements. With improved computational capacities, engineers in various fields have undertaken complicated modeling for structures under abnormal loads. However, an efficient and accurate model is necessary to more rapidly address dangerous shock problems. A relatively simple model will be detailed herein for the response prediction of the specific complex case of composite materials tested in a shock tube.

Thanks to superior properties, composite materials have replaced metals in various engineering applications. Composites offer numerous advantages such as high strength/weight ratio, low cost, corrosion performance, and improved stealth. Due to enhanced shock resistance, there is a specific demand for composite materials in defense applications. This investigation particularly relates to the usage on naval ships to achieve better blast survivability with the additional benefit of lower cost. While Gibson discussed the basic concepts, mechanical properties and test methods for composite materials in [1], shock damage evolution within a composite is still actively being investigated [2]. For instance, Bogdanovich applied geometrically nonlinear theory, dynamic

deformation, and failure analysis methods to laminated composite cylindrical shells exposed to longitudinal and lateral blast-type loading [3]. While these complex theories are useful, testing is still required to validate and verify model results.

Experimental investigations have been performed to induce shock damage in composite materials. Shock tests can be realized mainly by explosive or air blasts, both of which are costly and time-consuming. The more reusable test apparatus, shock tubes generate air shocks on specimens by using an inert gas either inside or outside a driving piston [4]. Utilized in this work, the shock tube constructed by Dr. Arun Shukla at the University of Rhode Island uses simply supported test specimens of 256 mm by 102 mm. The span of the experimental plate was 152 mm, and the overhangs were 50.8 mm at each end. Each specimen is placed into an instrumented driven section of the tube. In the adjoining driven section, helium pressure builds until a mylar diaphragm ruptures, sending an air blast that imparts a shock wave to the specimen [5].

Many researchers focus on finding computer models for such shock problems. Lall has developed an approach for analyze the shock damage initiation and progression, based on closed-form energy models, explicit finite elements, and statistical pattern [6]. Using a linear acoustic plane wave assumption, Li and Hua approximately solved the transient vibration of an elastic laminated composite cylindrical shell with infinite length exposed to an underwater shock wave [7]. Applying the finite element program Abaqus/Explicit together with a user material subroutine, large woven roving E-glass/vinyl-ester composite panels subjected to shock loads have also been modeled by Johnson *et al.* [8]. Through both three-dimensional X-ray microstructural investigation and a parallel series of shock experiments using a 50 mm ballistic gas gun, McDonald and Millett worked to link microstructure and simulation to predict the shock performance of a

composite material [9]. The propagating disturbance of breaking fibers has been generated by Goeke and McClintock to find the critical fracture location of three-dimensional graphite composites undergoing shock [10]. In a quite complicated manner, Raimondo *et al.* worked to join low velocity constitutive failure models, including delamination, with orthotropic state equations [11].

The main purpose of this paper is to obtain structural response to an arbitrary shock load through a modal analysis simulation, which is reasonably accurate and responsive as compared to complex models. Model input includes the gross properties of Young's modulus and material density as well as physical geometry and arbitrary shock load. Closed form equations have been employed to derive the eigenproblem that generates mode shapes and natural frequencies, and the aim is to estimate experimental responses of composite materials to actual shock tube results.

2 MODEL CASE STUDIES

Six different cases are used in this work to model a composite specimen's response to transient pressure. The modeled cases differ by applied load (Cases 1, 2, 3) and boundary conditions (Cases 4, 5, 6) in order to determine the most accurate model.

2.1 Description

Obtained via high-speed photography, a specimen view of the shock tube test configuration is shown in Figure 1. The longitudinal centerline section of the plate is simulated as a beam, and any transverse relative motion is neglected. Presuming linear elasticity, the employed Euler-Bernoulli beam model is provided in Figure 2. Permitting multiple boundary conditions, K_{t1} and K_{t2} are torsional springs while k_1 and k_2 are lateral springs. The width of the crossection is 101.6 millimeters, and the thickness is 9.525 millimeters. The gross material parameters used in the

simulation are provided in Table 1; note that the elastic modulus is determined through three-point bend beam impact testing at the University of Mississippi. Base excitation f(t) can be considered, but it is converted herein to an effective distributed force which simulates the shock tube pressure. Discrete test data has been provided for the mid-span displacement w(L/2, t) using optical means.

2.2 Case Studies

The applied impulse and boundary conditions are herein detailed for each simulated case.

2.2.1 Case 1

In Case 1, the entire excitation force is distributed over the entire beam length, as shown in Figure 3. This neglects that the exit tube does not extend over the free span and the plate overhangs the simple supports. Ideal pinned boundary conditions are also assumed.

The crossectional area of the shock tube at the 76.2 millimeter driven section A_{sec} is 4560.4 square millimeters. Thus, the excitation force F(t) is

$$F(t) = P(t)A_{sec} \quad ,$$

and the distributed pressure load q(t) is

$$q(t) = \frac{F(t)}{l} \quad .$$

Shown in Figure 4a, the applied pressure for Case 1 is simulated by dividing the measured pressure profile into two constant regions of average magnitude. Thus, the effective force is 21 and 19.25 Newtons per millimeter of beam length as shown in Figure 4b.

Modal analysis is employed to apply the equivalent force to the model. First, the closed-form beam equation is solved to obtain mode coefficients and natural frequencies. The first three calculated natural frequencies of the specimen VC00AS01 are 282.8 Hz, 1131.4 Hz, and 2545.5 Hz. For an exact solution, an infinite number of modes is required in the modal analysis, but

this is computationally unrealistic. Thus, convergence studies are employed to ensure that enough modes are used in the simulation. As provided in Figure 5, the results for this case converge at just two modes.

2.2.2 Case 2

In the actual shock tube tests, the ratio of the loading diameter to the span was the significant proportion of one-half as shown in Figure 6a. For Case 2, the distributed equivalent force is based upon the driven section diameter of three inches as provided in Figure 6b.

To evenly distribute the pressure over the entire beam, an equivalent deflection of Case 1 to Case 2 at the middle point is desired. The static mid-span deflection in Case 1 is

$$\delta_1 = \frac{5}{384}\frac{q_1 l^2}{EI},$$

and for Case 2 is

$$\delta_2 = \frac{11}{2048}\frac{q_2 l^2}{EI}.$$

In order to have the same deflection at the middle point, or $\delta_1 = \delta_2$, the equivalent distributed force is

$$q_1(t) = 0.4124\ q_2(t).$$

After applying this equivalence to the excitation of Case 1, the forces in Case 2 are shown in Figure 7.

2.2.3 Case 3

The effective excitation force for Case 3 is obtained in the same manner as in Case 2. However, the excitation pressure is discretized into smaller constant time intervals, as shown in Figure 8. The difference among Cases 1, 2 and 3 is strictly excitation force; thus, the models will converge

similarly.

2.2.4 Case 4

Case 4 is similar to Case 3 in excitation but has different boundary conditions. End moments are added to simulate the effect of the test specimens overhanging the supports.

As shown in Figure 9b, the moment induced is

$$M = \frac{1}{2}\rho A L^2 g = 13.6\ N - mm$$

,

where ρ is the material density, A is the cross sectional area of the plate, L is the length of the overhang, and g is gravitational acceleration. These moments are enforced as constant K_{t1} and K_{t2} (Fig. 2) and prove to be relatively small compared to the threshold of $1.13(10^8)$ N-mm/radians for fixed-fixed boundary conditions. The VC00AS01 Case 4 natural frequencies are less than 1% different from previous cases, and the response also converges at two modes.

2.2.5 Case 5

In Case 5, additional boundary conditions are considered. The supports were not attached to the specimens and relative motion may occur, specifically when pinned only on one side as in Figure 1. Thus, the values for the lateral springs k_1 and k_2 are adjusted to simulate this possible condition. With $1.8(10^5)$ N/mm being the threshold for pinned ends, both lateral spring constants of $1.8(10^3)$ N/mm were selected to allow limited motion. The first three natural frequencies of the specimen VC00AS01 are 267.1 Hz, 896.2 Hz, and 1572.6 Hz. With identical excitation force as in Case 4, convergence was again reached at two modes.

2.2.6 Case 6

For Case 6, possible asymmetric boundary conditions were simulated as differing the lateral spring constants k_1 and k_2 of $1.8(10^3)$ N/mm and $1.8(10^7)$ N/mm, respectively. The first three natural

frequencies of the specimen VC00AS01 are 274.5 Hz, 987.1 Hz, and 1878.7 Hz. The results for VC00AS01 Case 6 converge at two modes as well.

3 RESULTS

The six cases are plotted for VC00AS01 in Figure 10. Since Cases 3 and 4 are quite similar, the overhanging portions do not induce significant boundary changes. Case 1 shows a significantly greater deflection, indicating an overestimation of load. Case 1 is the most diverse as compared with all others; Case 2 through Case 6 are less than 5% different. As Case 5 is the most complex symmetric case, Cases 1 and 5 are used for further comparisons to experimental data. The results for the ten different materials are provided in Figures 11 through 20.

The results of the case studies as contrasted with the experimental shock tube results are provided in Table 2. In order to quantify the disparity, the root mean square (RMS) relative difference of the model (y) to the test (x) response was calculated by

$$\sqrt{\frac{1}{n}\sum_{i=1}^{n}\left(\frac{y_i - x_i}{x_i}\right)^2}$$

where n is the number of discrete data points.

4 DISCUSSION

As discussed in the following subsections, three main conclusions can be characterized from these results. Note that the peak pressure in the shock tube was approximately 0.5 MPa and faded over 14 milliseconds, inducing an average velocity of approximately 6 m/s in the specimens.

4.1 Case 1 Applicability

Unexpectedly, the simplest case is the most accurate for broken specimens. Case 1 is a reasonable model for all fractured specimens with nanoreinforcement. This may be because using an elastic

model does not consider the plastic deformation of the specimen. The consideration of the shock impulse spanning the entire beam compensates for the neglect of plasticity in the model. Similar results were obtained as well in the impact tests of [12]. For the unbroken specimens, it is not clear which case is a better model as it depends on whether the specimen has entered the plastic range. In short, Case 1 is an advisable model choice for response approximation for any case: the result is a conservative overestimate of deflection.

4.2 Case 5 Underestimation

For most cases, the model underestimates the deflection. This implies that either the force is underestimated or the plate stiffness may be overestimated. Another possible explanation is that, although the driver section is close to contacting the specimen, leakage may exist which could allow the pressure pulse to spread to other areas besides the driver section. This would have a considerable effect as the linear model is quite sensitive to the applied force. Additionally, the beam model does not consider any transverse or directional plate properties. The layup of the E-glass fibers is also neglected as the gross material properties are employed.

4.3 Frequency Underestimation

For every experimental test, the measured data points reveal an upward trend before 1.75 milliseconds have elapsed. The rebounding behavior implies that the model underestimates the natural frequencies of the plate. While this could be due to transverse modal coupling, the gross elastic modulus is a more likely cause. As it is universally proportional to the model's natural frequencies, the elastic modulus measured by the impact machine may undervalue the effective modulus in the shock tube tests. The results of a parameter study for the unreinforced specimen VC00AS01 is shown in Figure 21. Case 1 shows the best agreement with the test data when the

modulus used for the simulation is 1.75 times bigger of the given value. Note that another source of higher frequencies may be contact with the supports, which will be examined in the future. Case 5 provides the same trend but does not improve its accordance as the elastic modulus increases.

5 SUMMARY

The structural response to an arbitrary shock load has been obtained through a modal analysis simulation. Model input includes the gross material properties, physical geometry, and shock tube pressure. Closed form equations have been employed to generate the mode shapes and natural frequencies that correspond to ten different composite material configurations. After considering a variety of boundary conditions and impulse discretizations, simulation responses show that a uniform full-span load generated from an averaged pressure model provides a fairly accurate model. This case specifically applies for all fractured specimens with reinforcement, and it is an advisable and conservative choice for all other specimens as well. The model is strictly linear; however, the specimens enter a nonlinear plasticity or fracture state. All specimens are composite, so an isotropic beam model will result in additional disparity. Despite these simplifications, the results with the closed-form beam model are similar in range with the experimental results. Thus, this quick and efficient tool estimates experimental shock tube test response with reasonable accordance.

6 ACKNOWLEDGMENTS

The research was funded by ONR Grant #N00014-07-1010, Office of Naval Research, Solid Mechanics Program (Dr. Yapa D.S. Rajapakse, Program Manager). We would like to thank Dr. Arun Shukla at the University of Rhode Island for performing the shock tube tests.

REFERENCES

[1] Gibson, R. F., 2007, Principles of Composite Material Mechanics (2nd edition), CRC Press.

[2] Tekalur, S. A., Shivakumar, K., and Shukla, A., 2008, "Mechanical behavior and damage evolution in E-glass /vinyl-ester and carbon composites subjected to static and blast loads," Composites: Part B, 39, pp. 57–65.

[3] Bogdanovich, A., 1993, "Non-linear Dynamic Problems for Composite Cylindrical Shells," London, New York: Elsevier Applied Science,.

[4] Glenn, D. H., and Croeley, B. K., April 1971, "Analysis of a high-explosive shock-tube experiment," Journal of Applied Physics, 42(5), pp. 2099-2105.

[5] Tekalur, S. A., Shukla, A., and Shivakumar, K., 2008, "Blast resistance of polyurea based layered composite materials," Composite Structures, 84, pp. 271-281.

[6] Lall, P., Choudhary, P., Gupte, S., and Suhling, J., 2006, "Health monitoring for damage initiation & progression during mechanical shock in electronic assemblies," 2006 Electronic Components and Technology Conference, San Diego, California USA, pp. 85-94.

[7] Li, J., and Hua, H., 2009, "Transient vibration of laminated composite cylindrical shells exposed to underwater shock waves," Engineering Structures, 31, pp. 738-748.

[8] Johnson, H. E., Louca, L. A., and Mouring, S. E., 2006, "Current research into modeling of shock damage to large scale composite panels," Journal of Material Science, 41, pp. 6655–6672.

[9] McDonald, S. A., and Millett, J. C. F., 2007, "The shock response, simulation and microstructural determination of a model composite material," Journal of Material Science, 42, pp. 9671–9678.

[10] Goeke, E. C., and McClintock, F. A., 1975, “Fracture of graphite composites under shock loading,” Journal of Applied Physics, 46(11), pp. 4671-4673.

[11] Raimondo, L., Lannucci, L., Robinson, P., Curtis, P. T., and Wells, C. M., 2005, “Shock modeling of multi-phase materials: advances and challenges,” 2005 ASME Pressure Vessels and Piping Division Conference, Denver, Colorado USA, pp. 807-817.

[12] Mouring, S. E., Louca, L., and Levis, W., 2005, “Structural response of impact-damaged composite panels,” Proceedings of MTS/IEEE OCEANS 2005, 2, pp. 1370 - 1373.

LIST OF TABLE CAPTIONS

Table 1. Measured E-glass/vinyl-ester specimen properties.

Table 2. RMS comparison of model to data and resulting conclusions.

LIST OF FIGURE CAPTIONS

Table 1. Measured E-glass/vinyl-ester specimen properties.

Sample Name	Reinforcement	Density (kg/m^3)	Flexural Modulus (GPa)	Weight %
VC00AS01	None	1112.44	2.56	-
VC00AS01t2	None			-
VC12BS01	NanoClay	1132.99	2.24	1.25%
VC12BS02				
VC25BS01		1139.65	2.55	2.5%
VC25BS02				
VG12BS01	Graphite Platelets	1117.29	2.73	1.25%
VG12BS02				
VG25BS01		1133.58	3.56	2.5%
VG25BS02				

Table 2. RMS comparison of model to data and resulting conclusions.

Sample Name	Post Test Condition (Load)	RMS Difference		Applicable Section(s)
		Case 1	Case 5	
VC00AS01	unbroken (0.48 MPa)	0.648	0.624	4.2, 4.3
VC00AS01t2	broken (0.83 MPa)	1.540	0.509	4.2, 4.3
VC12BS01	unbroken (0.48 MPa)	0.959	0.619	4.2, 4.3
VC12BS02	broken (0.83 MPa)	0.374	0.718	4.1
VC25BS01	unbroken (0.48 MPa)	1.104	0.593	4.2, 4.3
VC25BS02	broken (0.83 MPa)	0.734	0.898	4.1, 4.2
VG12BS01	unbroken (0.48 MPa)	0.563	0.579	4.2, 4.3
VG12BS02	broken (0.83 MPa)	0.402	0.746	4.1
VG25BS01	unbroken (0.48 MPa)	0.585	0.716	4.2, 4.3
VG25BS02	broken (0.83 MPa)	0.631	0.929	4.1

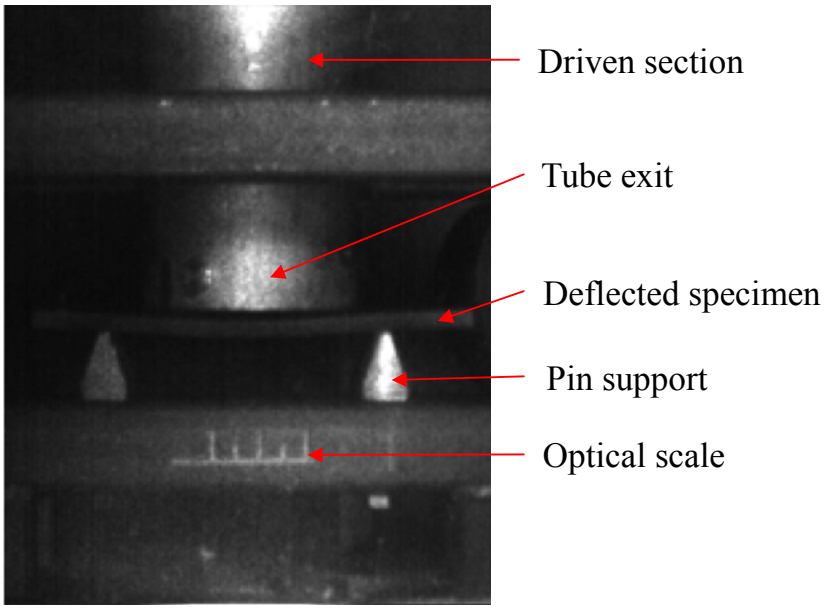

Figure 1. A still photograph of a loaded test specimen.

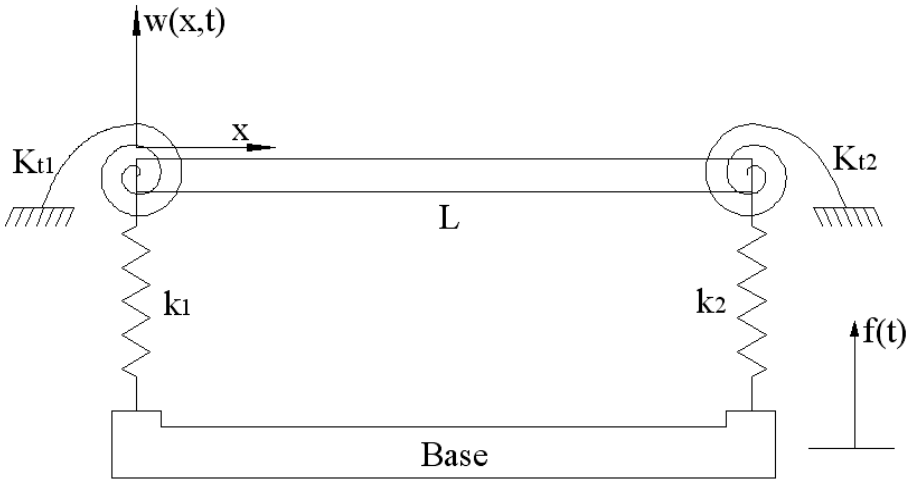

Figure 2. First principles beam model.

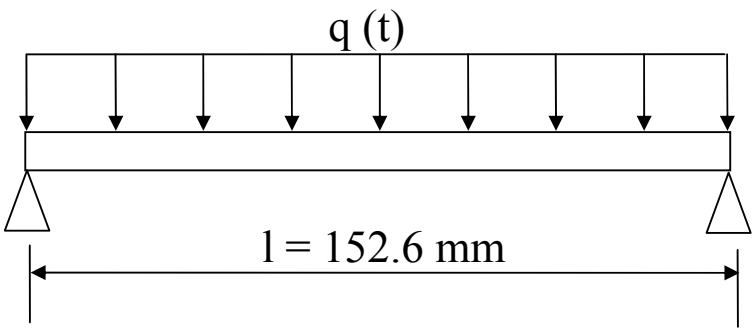

Figure 3. Distributed load model of Case 1.

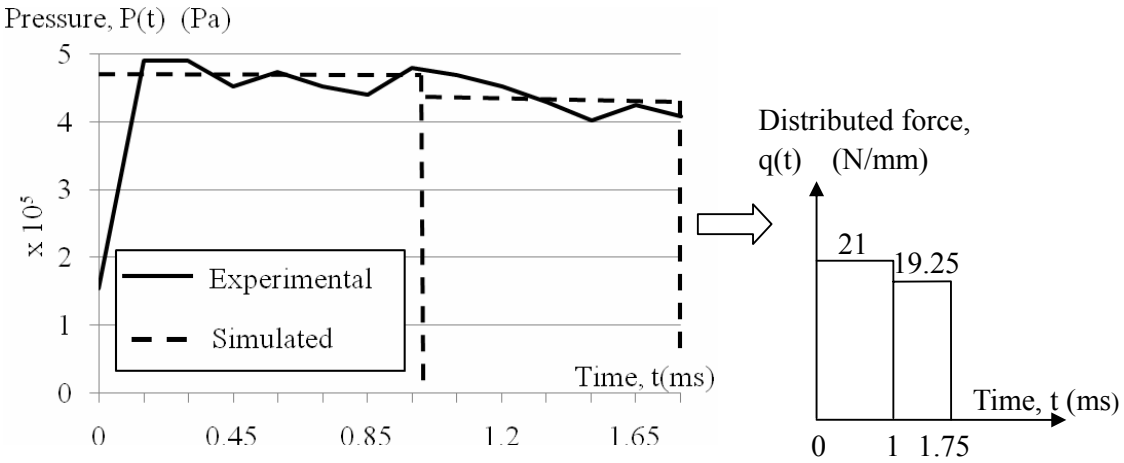

Figure 4. (a) Applied pressure P(t) and (b) excitation force for VC00AS01 Case 1.

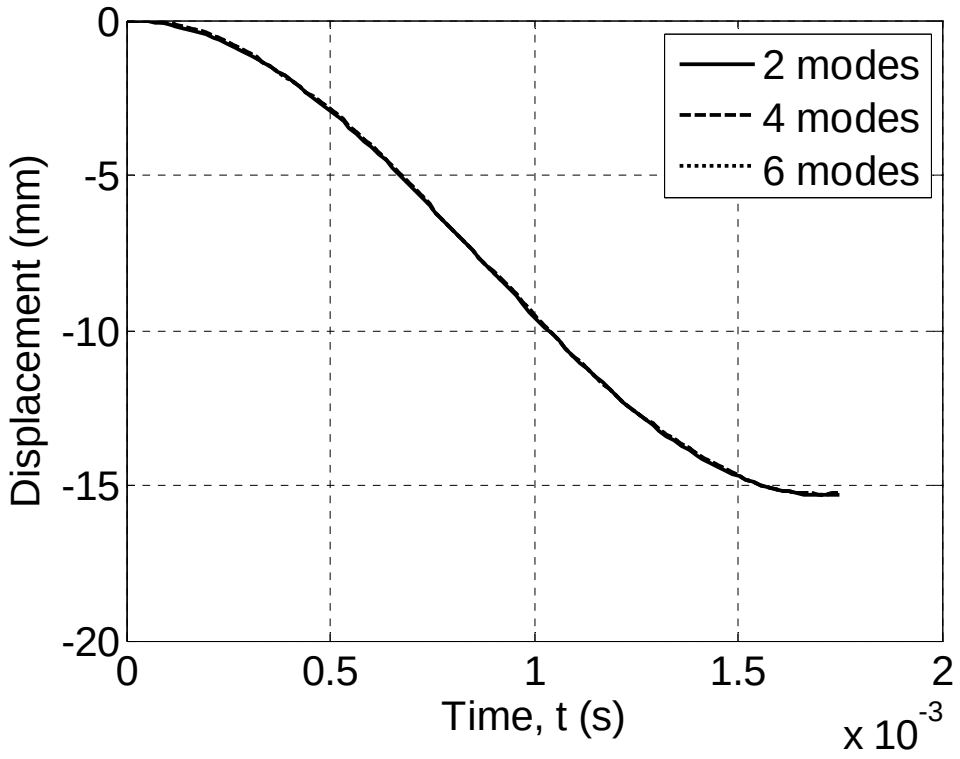

Figure 5. Convergence study for VC00AS01 Case 1.

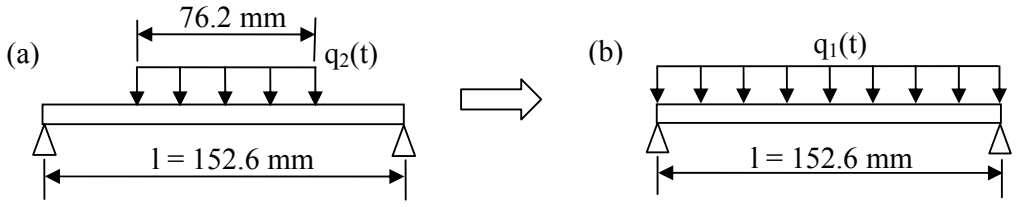

Figure 6. Configuration of (a) experimental specimen and (b) simulated model.

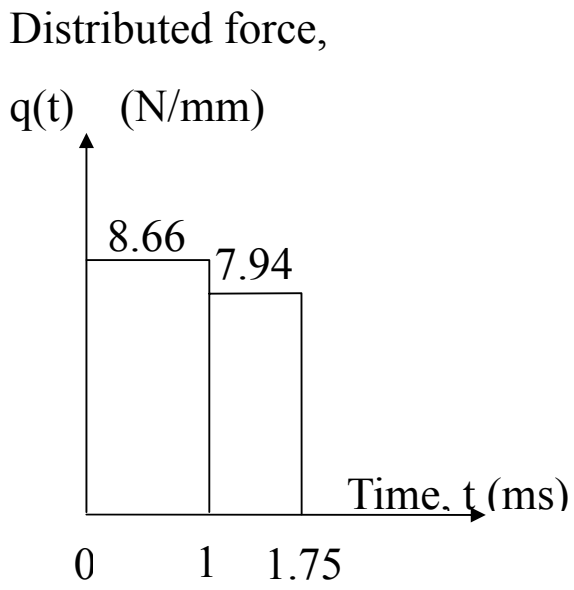

Figure 7. Equivalent force values for Case 2.

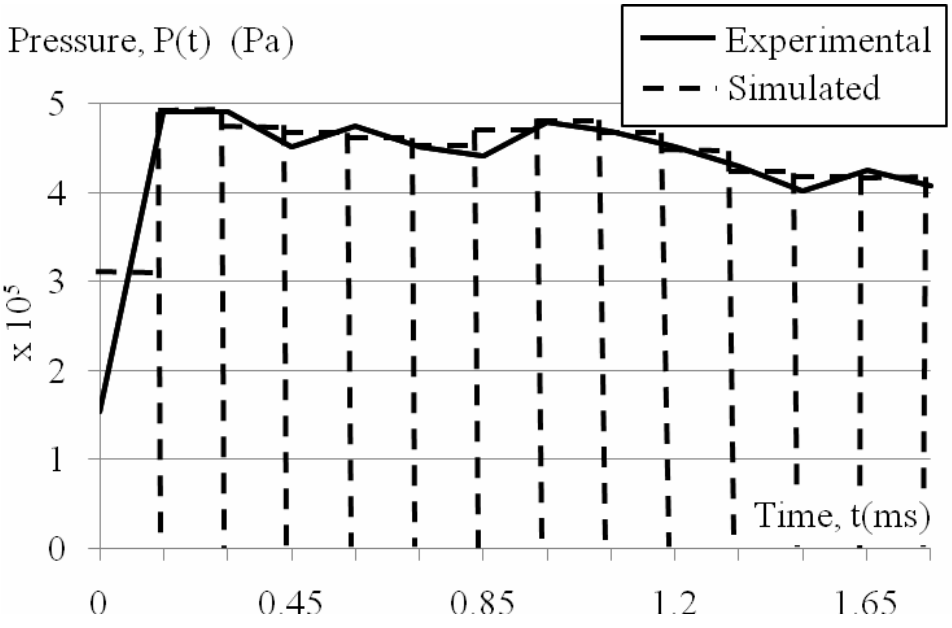

Figure 8. Excitation pressure for VC00AS01 Case 3.

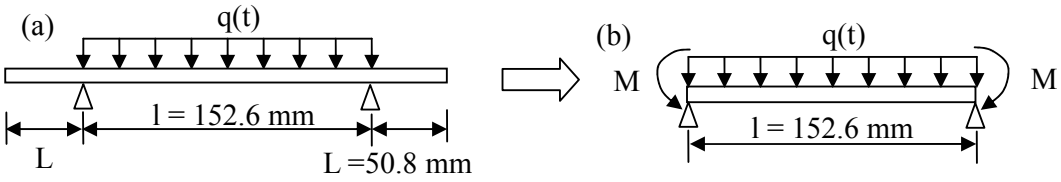

Figure 9. Beam model for Case 4.

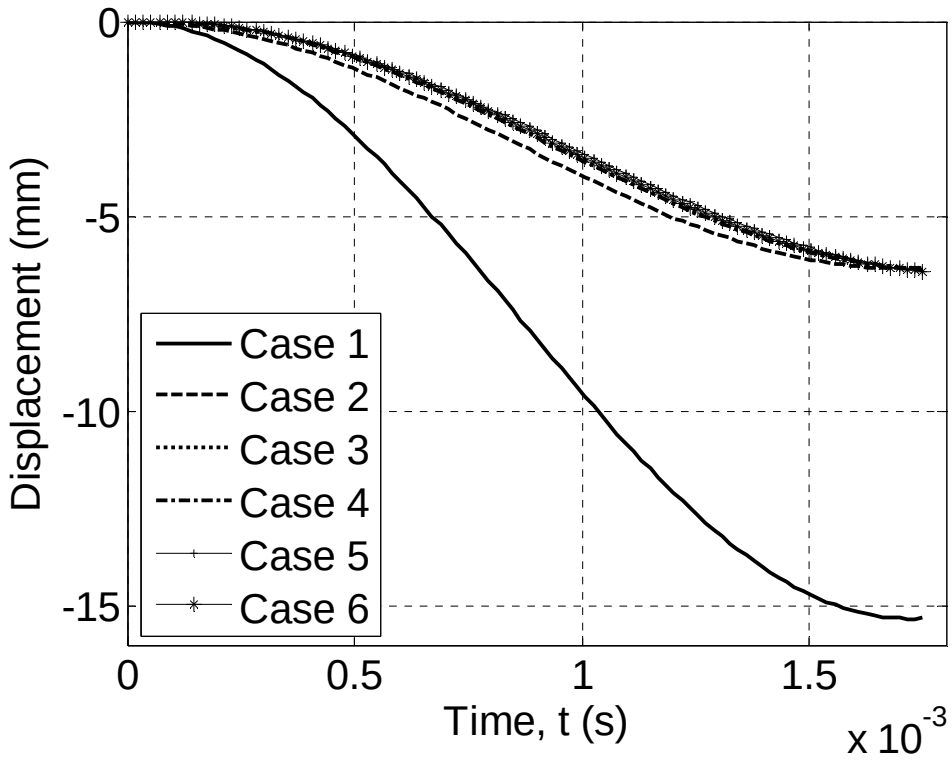

Figure 10. Comparison of the mid-span deflection of the six cases for VC00AS01.

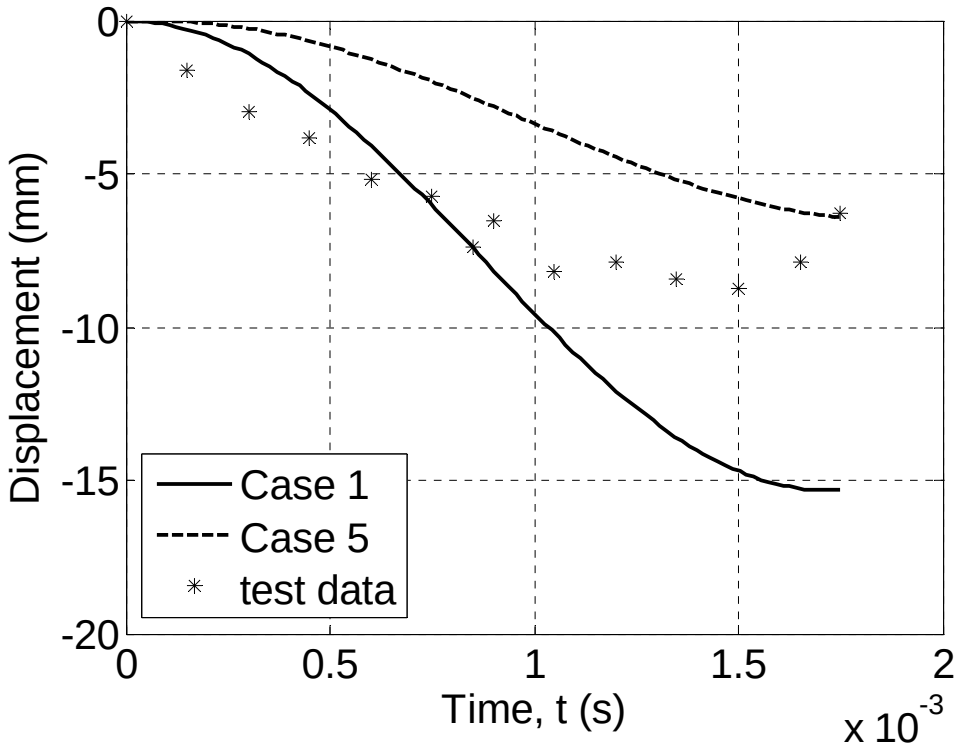

Figure 11. Mid-span deflection for VC00AS01.

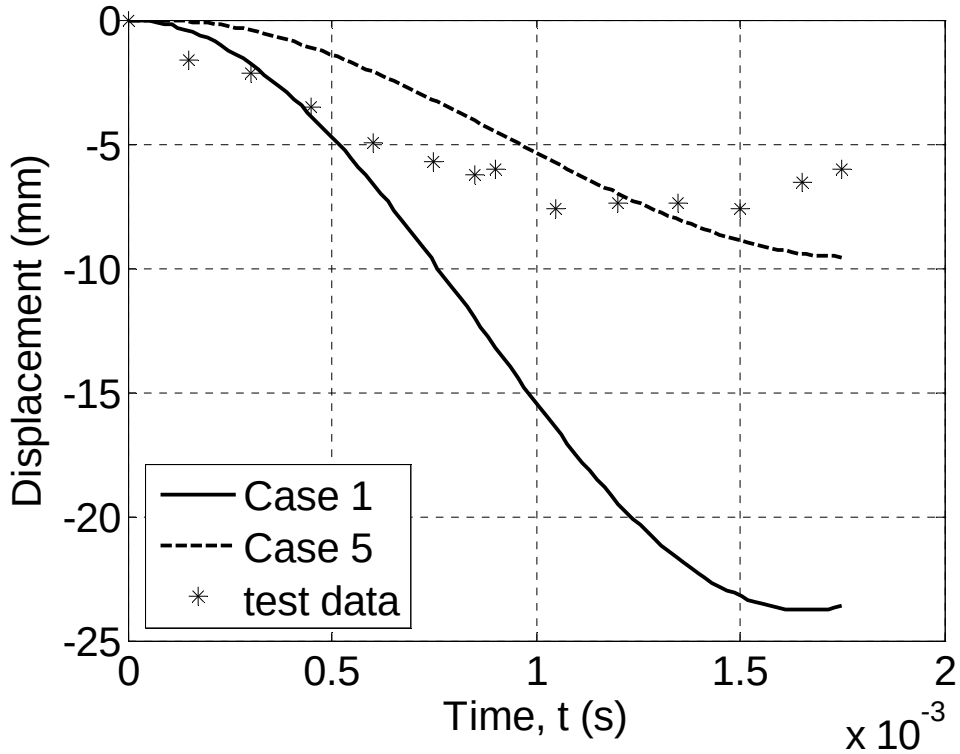

Figure 12. Mid-span deflection for VC00AS01t2.

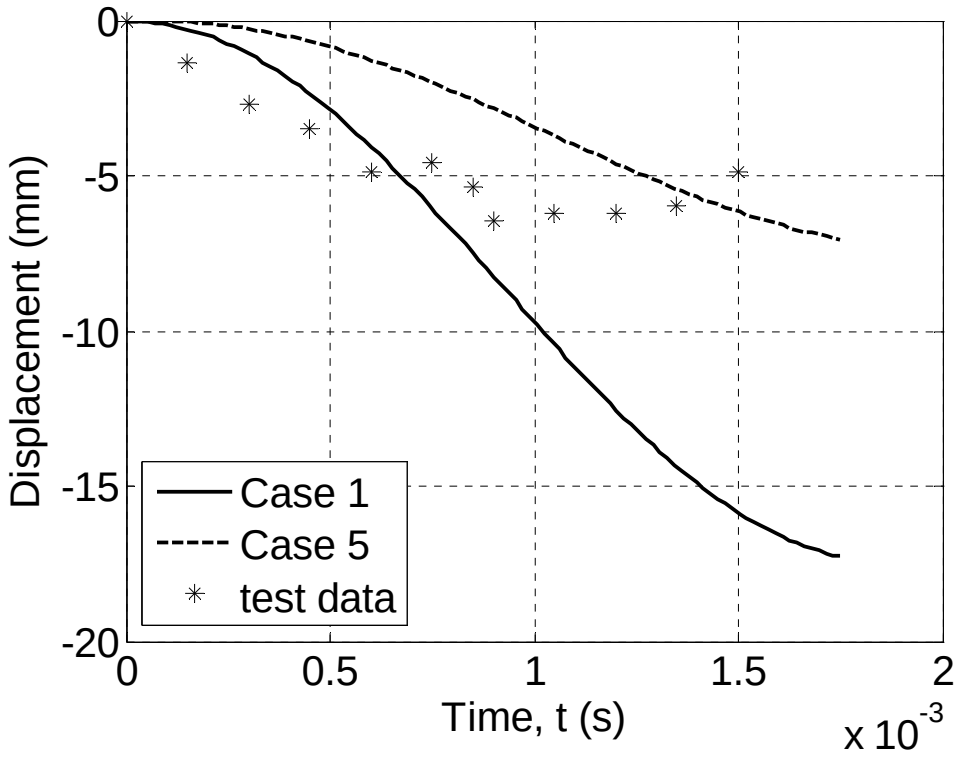

Figure 13. Mid-span deflection for VC12BS01.

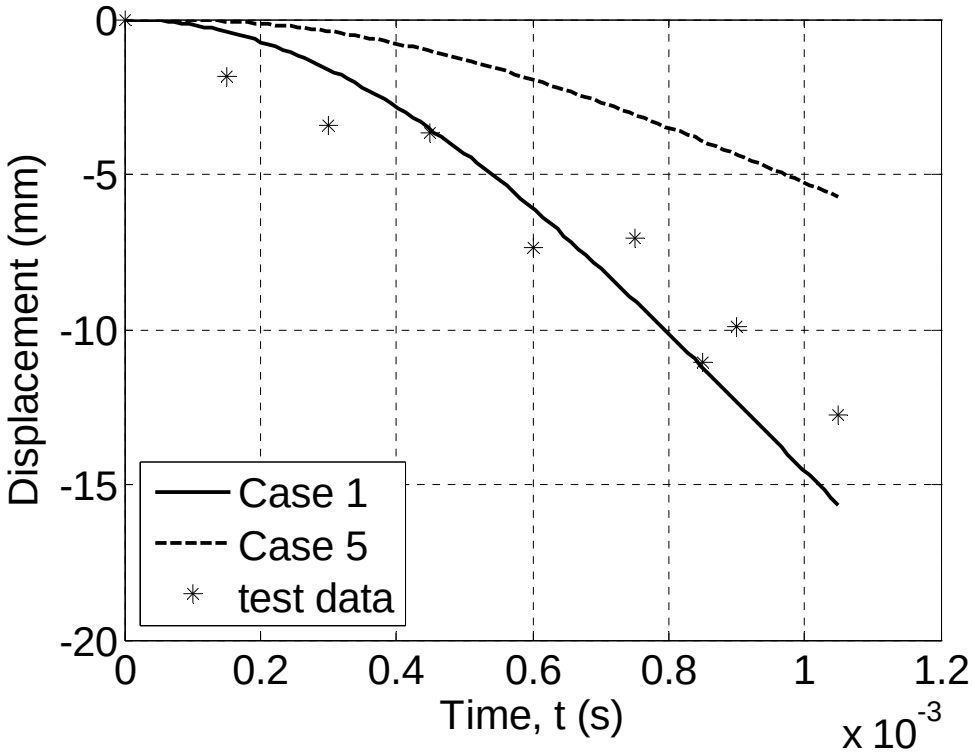

Figure 14. Mid-span deflection for VC12BS02.

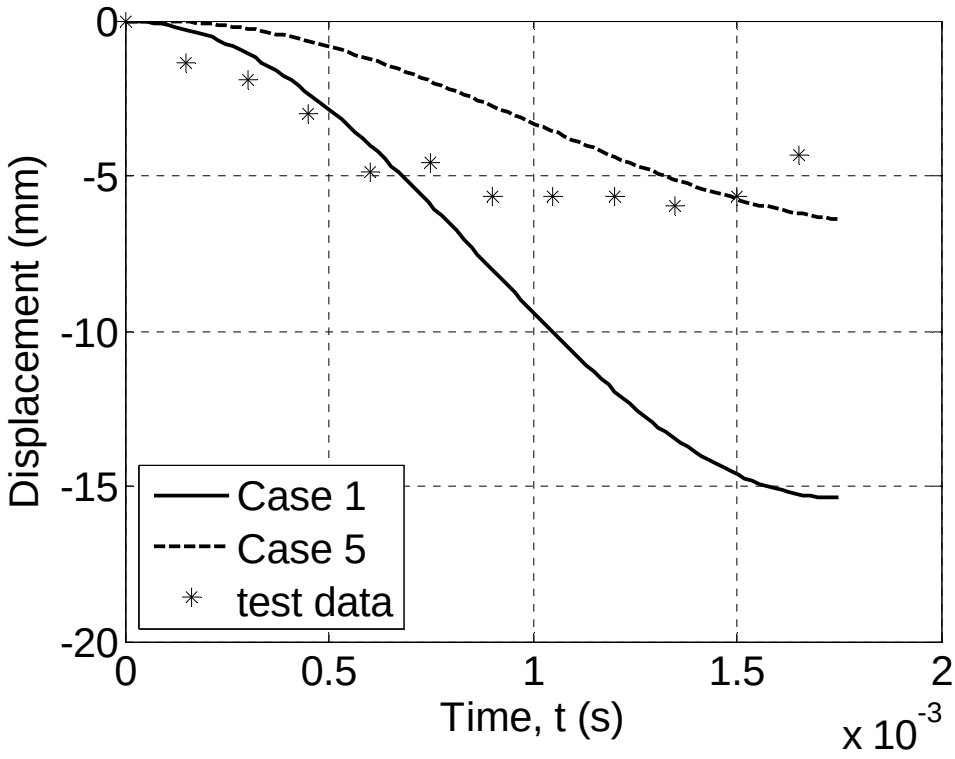

Figure 15. Mid-span deflection for VC25BS01.

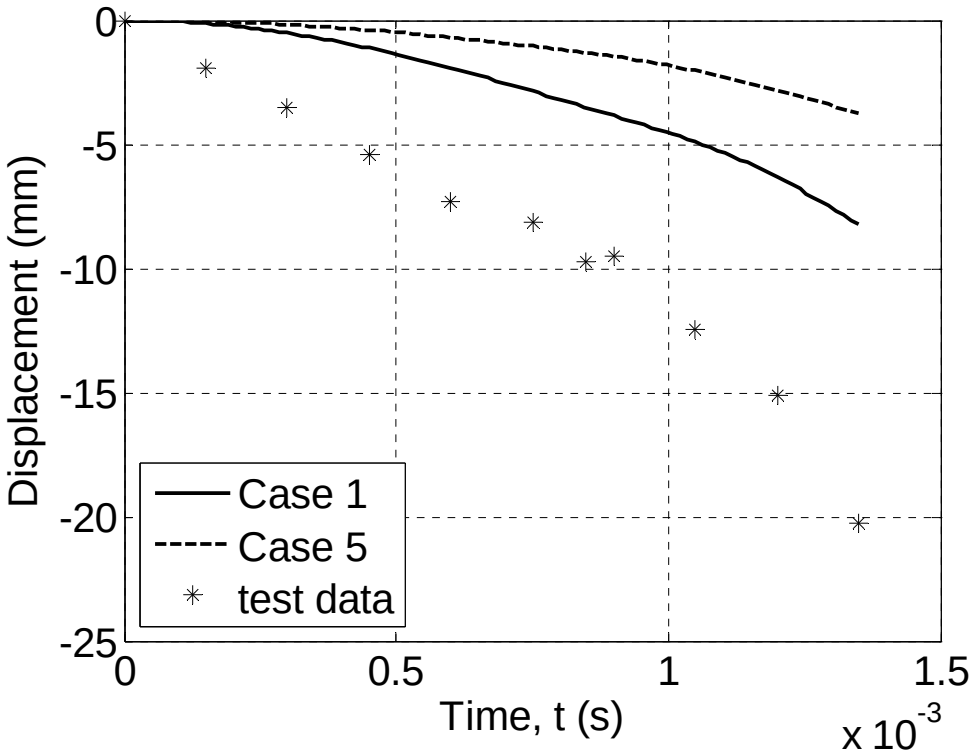

Figure 16. Mid-span deflection for VC25BS02.

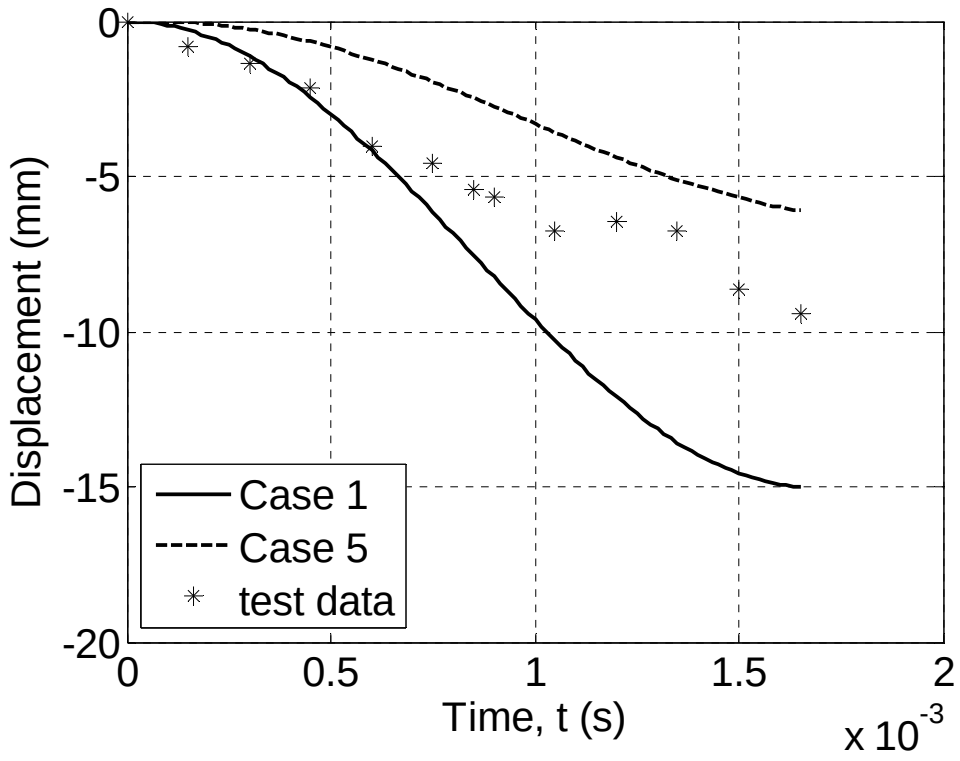

Figure 17. Mid-span deflection for VG12BS01.

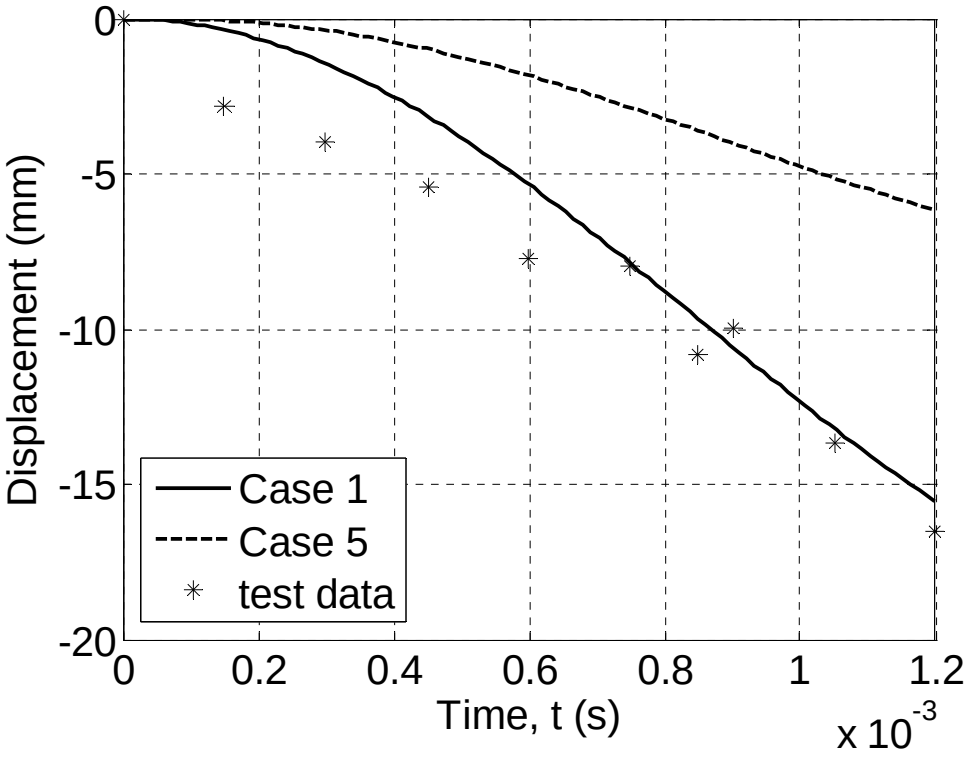

Figure 18. Mid-span deflection for VG12BS02.

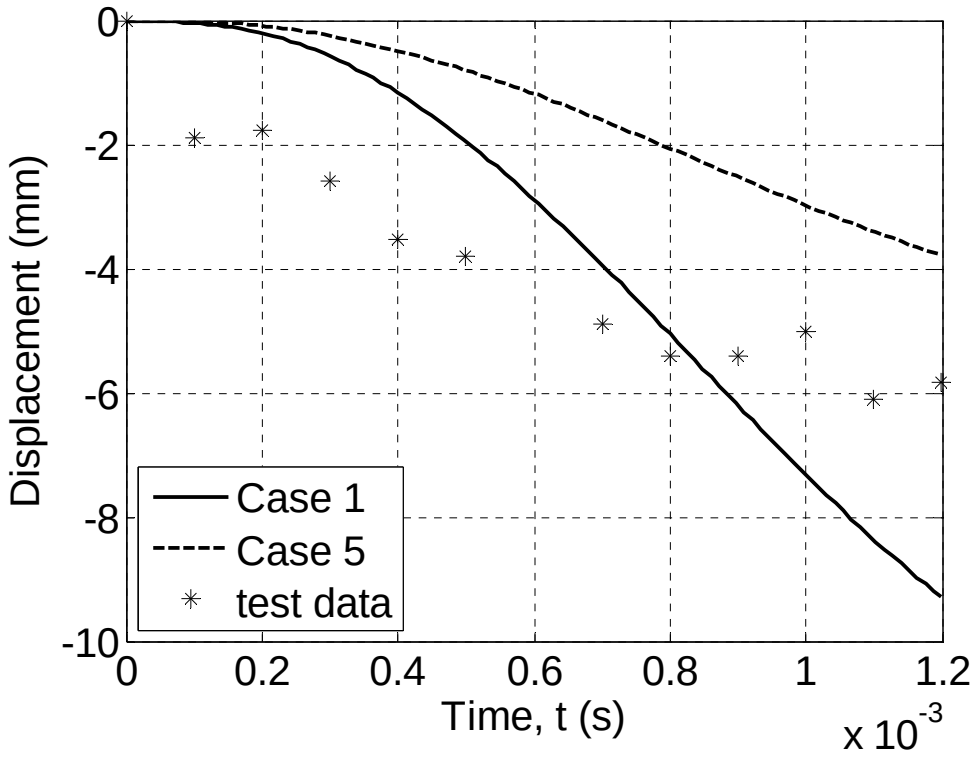

Figure 19. Mid-span deflection for VG25BS01.

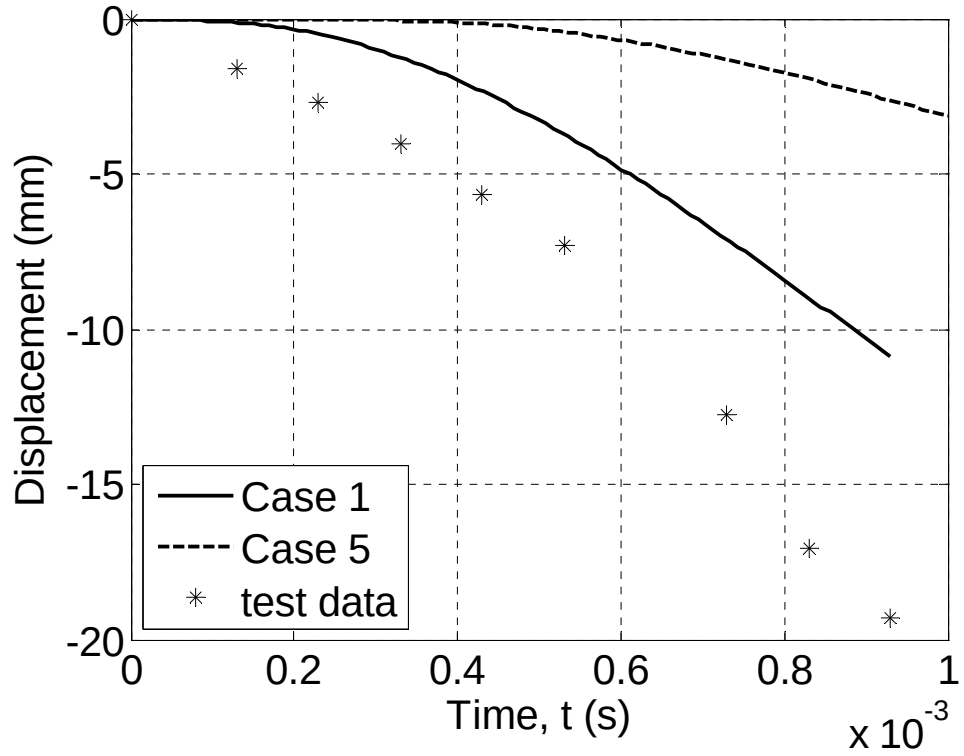

Figure 20. Mid-span deflection for VG25BS02.

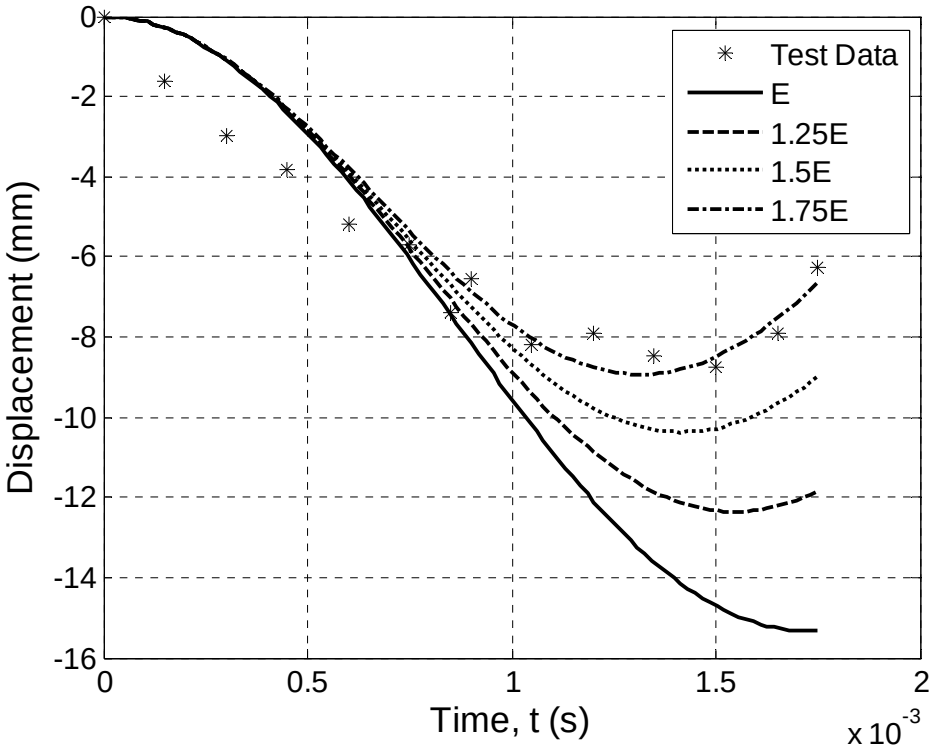

Figure 21. Mid-span displacement of Case 1 VC00AS01 with changing elastic modulus.